

碩士學位論文

Dynamic Electrical Impedance Tomography with Prior Information

濟州大學校大學院



姜 淑 仁


2002年 12月

Dynamic Electrical Impedance Tomography with Prior Information

指導教授 金 慶 淵
姜 淑 仁

이 論文을 工學 碩士學位 論文으로 提出함

2002年 12月

 제주대학교 중앙도서관
姜淑仁의 工學 碩士學位 論文을 認准함

審査委員長 _____ (印)

委 員 _____ (印)

委 員 _____ (印)

濟州大學校 大學院

2002年 12月

Dynamic Electrical Impedance Tomography
with Prior Information

Suk In Kang

(Supervised by professor Kyung-Youn Kim)



A THESIS SUBMITTED IN PARTIAL FULFILLMENT OF THE
REQUIREMENT FOR THE DEGREE OF MASTER OF ENGINEERING

2002. 12

DEPARTMENT OF ELECTRICAL AND ELECTRONIC
ENGINEERING, GRADUATE SCHOOL
CHEJU NATIONAL UNIVERSITY

Contents

Summary (in Korean)	1
I Introduction	2
II Image reconstruction methods in EIT	6
2.1 Forward solver for the physical model of EIT	7
2.2 Inverse solver for the image reconstruction	10
2.2.1 Modified Newton-Rapson method (mNR)	11
2.2.2 Modified Newton-Rapson method with Tikhonov regularization	12
2.2.3 Extended Kalman filter	13
2.2.4 Calculation of Jacobian	17
III Dynamical electrical impedance tomography with prior information	19
3.1 Partially known internal structure & resistivity (EKF-SR)	20
3.2 Internal electrode attached to the known internal structure (EKF-IE)	22
IV Computer simulations & experimental results	23
4.1 Partially known internal structure & resistivity	23
4.1.1 Computer simulation results	24
4.1.2 Experimental results	25
4.1.3 Errors in the reconstructions	27
4.1.4 Effects of parameter values (α, β) on the reconstruction performance	27
4.2 Internal electrode attached to the known internal structure	30
4.2.1 The first simulation results	32
4.2.2 The second simulation results	32
4.2.3 Effects of parameter value (α) on the reconstruction performance	33
4.2.4 Effects of the measurement and linearization error on the reconstruction performance	33
V Conclusions	36
Summary	37
References	38

초 록

전기 임피던스 단층촬영법(electrical impedance tomography)은 물체의 경계면의 전극에서 전류를 주입하여 얻은 측정 전압으로, 물체 내부의 저항률 분포에 대한 영상을 비파괴적으로 복원하는 기법이다.

지금까지 연구의 대부분은 1 프레임(frame)의 전압 측정치를 얻는 동안 물체 내부의 저항률 분포가 변하지 않는 정적(static) 영상복원에 관한 것이었다. 본 연구는 1 프레임의 전압 측정치를 얻는 동안에 물체 내부의 저항률 분포가 급변하는 동적(dynamic) 영상복원에 관한 것으로서, 특히 영상복원 전에 사전에 알고 있는 정보를 효과적으로 이용함으로써 복원된 영상의 성능을 개선하고자 한다. 즉 실제의 화학 공정과 같은 물체에 대한 사전(prior) 정보를 갖는 경우처럼, 목표물의 중앙부에 사전 정보를 갖는 고전도성 물체가 존재하고 그 물체 외 영역의 저항률이 급변하는 경우를 고려하였다. 이 경우에 고전도성 물체와 타겟이 서로 가까워지면, 저항률이 고대비(high contrast)를 이룬다. 고대비로 인한 타겟 부위의 내부 전류 밀도는 조밀(dense)하지 못하고, 이는 차폐현상(making effect)을 발생하여 기존의 알고리즘으로는 영상복원을 어렵게 한다.

따라서, 본 논문에서는, 시간에 따라 변화는 저항률 분포를 온라인으로 추정하고 차폐현상을 완화하기 위해, 목표물 중앙부의 고전도성 물체에 대한 위치 및 저항률의 사전 정보를 이용하여 최적화 문제의 비용함수에 추가시켜 영상복원 성능을 개선하는 기법과, 고전도성 물체를 내부 전극으로 사용하여 전류를 주입함으로써 내부 전류 밀도를 향상시켜 영상복원 성능을 개선하는 두 가지 기법을 개발하였다.

본 논문에서 제안된 영상복원 기법의 성능을 검증하기 위해 컴퓨터 시뮬레이션 및 실험 결과를 제시하였다. 결과적으로 제안된 영상복원 기법에서는 차폐현상을 완화하여 복원된 영상의 시간해상도 및 공간해상도를 개선할 수 있음을 보였다.

I. Introduction

Initially, electrical tomography (ET) technique has been developed as alternatives to the medical imaging techniques such as X-ray imaging, computerized tomography (CT), gamma camera, magnetic resonance imaging (MRI) and ultrasonic imaging, some of which are expensive and/or even cause adverse health impacts. Since ET is characterized by good time resolution and low cost, it has obvious advantages in the application to the medical imaging and visualization of two-phase flow systems (Webster, 1990), (Williams & Beck, 1995), (Cheney et al, 1999).

If the electromagnetic properties of different materials inside the object differs from each other the spatial and/or temporal distributions of the material properties can be estimated based on the various ET techniques. In general, the ET techniques can be classified into three categories according to the electromagnetic quantities to be imaged; These quantities are the magnetic permeability (μ), electric permittivity (ϵ) and electric conductivity (σ), which correspond to electromagnetic inductance tomography (EMIT) (Peyton et al,1996), electrical capacitance tomography (ECT) (Xie et al 1992) and electrical resistance tomography (ERT) (Dickin & Wang, 1996), respectively. In all of the above tomographic techniques, the relationships between the electromagnetic quantities inside the object and sensing quantities on the surface are described by the Maxwell's equations (Webster, 1990).

In electrical impedance tomography (EIT), the quantity to be imaged is actually the impedivity (inverse of admittivity) so that it includes both ECT and ERT. However, more frequently in EIT it assumed that the resistive part of the impedivity dominates and estimates only the resistivity (inverse of conductivity) distribution inside the object. In EIT, the internal resistivity distribution is reconstructed based on the known sets of injected currents and measured voltages on the surface of the object. The physical relationship between the internal resistivity and the surface voltages is governed by a partial differential equation (Laplace equation) with appropriate boundary conditions. Owing to the complexity of this relationship, it is in

most cases impossible to obtain a closed-form solution for the resistivity distribution. Hence, various reconstruction algorithms have been developed in the literature to estimate the internal resistivity distribution of the object.

However, most of the reconstruction algorithms presented so far are mainly focused on the case where the internal resistivity of the object is time-invariant within the time taken to acquire a full set of independent measurement data. As is well known, the conventional EIT imaging techniques such as backprojection or modified Newton-Raphson (mNR) algorithm use a full set of voltage measurements for each image (Barber & Brown, 1984), (Yorkey et al, 1987). However, in real applications such as biomedical and chemical processes, these static imaging techniques are often fail to obtain satisfactory temporal resolution for the reconstructed images due to the rapid changes in resistivity.

More recently, dynamic imaging techniques have been developed to enhance the temporal resolution of the reconstructed images in the situations where the resistivity distribution inside the object changes rapidly in time. In most of these techniques, the inverse reconstruction problem is treated as state estimation problem and the time-varying state is estimated with the aid of linearized Kalman filter (LKF) (Vauhkonen et al, 1997, 1998, 2000) or extended Kalman filter (EKF) (Kim et al, 2001). Although the LKF has the computational advantage that the Kalman gain can be precomputed off-line and stored in a memory since the observation equation is normally linearized about the nominal value or the best homogeneous resistivity which is computed based on a set of voltage measurements, the rationale for the choice of the EKF instead of the LKF is that the linearization state for the LKF is usually not as close to the actual trajectory as is the predicted state used in the EKF. Therefore, the EKF may have improved reconstruction performance especially in the situations in which the resistivity distribution changes greatly from the assumed linearization state. The improvement is obtained with the expense of slightly increased computational burden that is due to the updating the electrode voltages and the Jacobian for each iteration. The detailed comparison between LKF and EKF in EIT imaging is appeared in (Kim et al, 2001).

Quite often in real situations there are partially known fixed internal structures and/or resistivities inside the object. These internal structures can be, for example,

an impeller drive shaft or a mixing paddle in process vessels and an assembly of fuel rods in nuclear reactor. The internal structures inside the object may result in difficulties in the image reconstruction in EIT especially in the case where the high resistive region is near the conductive internal structure (Heikkinen et al, 2001). The so-called masking effect in the reconstructed image may be significant for the high-contrast case. There are two ways to get around these difficulties; the one is to take into account it as *a priori* information in the inverse procedure (Heikkinen et al, 2001) and the other is to use the internal structure as additional electrodes (Lyon & Oakley, 1993), (Heikkinen et al, 2001). However, all of the above approaches are for the case where the resistivity distribution inside the object is time-invariant for one classical frame.

The objective of this thesis is to develop a dynamic EIT reconstruction algorithm for the case where the fixed internal structure and/or its resistivity are known partially and the resistivity distribution of the other part inside the object changes rapidly within the time taken to acquire a full set of independent measurement data. Special attention is given to use the known internal structure and/or resistivity as *a priori* information. In the first method an additional constraint for the known internal structure and/or its resistivity is incorporated into the cost functional as *a priori* information and in the second method the internal electrode is attached to the internal structure in addition to the external electrodes. In two proposed methods the inverse problem is treated as the state estimation problem and the unknown state (resistivity) is estimated with the aid of the EKF in a minimum mean square error sense. In order to deal with the well known ill-posedness of the EIT inverse problem, smoothness assumption is made and the modified Tikhonov regularization technique is also introduced in the cost functional.

We carried out both computer simulations with synthetic data and laboratory experiment with real measurement data extensively to illustrate the reconstruction performance, and to investigate the effects of *a priori* information on the spatial and temporal resolution for the assumed scenarios.

The thesis is organized as follows. After introduction in chapter I, a short review on the reconstruction algorithm widely used in EIT for the static or dynamic reconstruction is given in chapter II. The proposed algorithms are appeared in chapter

III. In chapter IV, computer simulations and experimental results are given to illustrate the effects of *a priori* information on the spatial and temporal reconstruction performance. Conclusions are given in the final chapter.



II. Image reconstruction methods in EIT

EIT is a relatively new imaging modality in which the internal impedivity distribution is reconstructed based on the known sets of injected currents and measured voltages on the array of electrodes which are attached on the boundary of an object. The concept of EIT is depicted in Fig. 2.1.

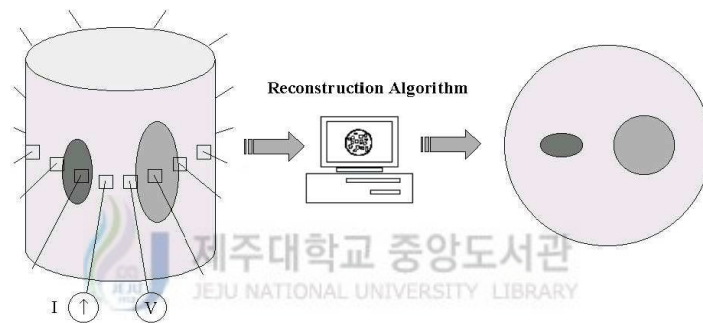


Fig. 2.1. Concept of electrical impedance tomography

Image reconstruction in EIT is obtained by iteratively solving the forward problem and inverse problem. In the forward problem, boundary voltages are calculated by using the assumed resistivity distribution. On the contrary, in the inverse problem, resistivity distribution is estimated by using the boundary voltage measurements. Brief concept of forward and inverse problems is depicted in Fig. 2.2.

The EIT reconstruction problem is a nonlinear ill-posed inverse problem. To solve the EIT inverse problem, many different reconstruction algorithms have been proposed in the literature. One of the most common is the minimization of the squared norm of the difference between the calculated voltages and the measured voltages on the boundary electrodes. However, because of the ill-posed nature of the problem, the minimization has to be regularized in order to obtain stable solution.

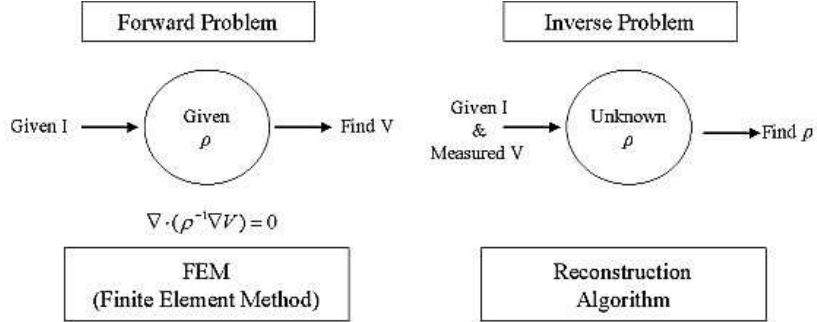


Fig. 2.2. Forward vs. inverse problem in EIT

In section 2.1 we formulate the EIT forward problem based on the complete electrode model (CEM) (Cheng et al, 1989),(Vauhkonen, 1997) and describe the numerical solver by the finite element method (FEM). The inverse solver based on the mNR and the EKF is presented in section 2.2.

2.1 Forward solver for the physical model of EIT

When electrical currents $I_l (l = 1, 2, \dots, L)$ are injected into the two-dimensional object Ω through the electrodes $e_l (l = 1, 2, \dots, L)$ attached on the boundary $\partial\Omega$ and the resistivity distribution $\rho(x, y)$ is known for the Ω , the corresponding electrical potential $u(x, y)$ on the Ω can be determined uniquely from the partial differential equation, which can be derived from the Maxwell equations:

$$\nabla(\rho^{-1}\nabla u) = 0 \quad \text{in } \Omega \quad (2.1)$$

with the following boundary conditions based on the complete electrode model :

$$u + z_l \rho^{-1} \frac{\partial u}{\partial n} = U_l \quad \text{on } e_l, l = 1, 2, \dots, L \quad (2.2)$$

$$\int_{e_l} \rho^{-1} \frac{\partial u}{\partial n} dS = I_l, \quad l = 1, 2, \dots, L \quad (2.3)$$

$$\rho^{-1} \frac{\partial u}{\partial n} = 0 \quad \text{on} \quad \partial\Omega \setminus \bigcup_{l=1}^L e_l \quad (2.4)$$

where z_l is the effective contact impedance between l th electrode and electrolyte, U_l is the potential on the l th electrode, e_l is l th electrode, n is outward unit normal, L is number of electrodes, and $\partial\Omega \setminus \bigcup_{l=1}^L e_l$ is the boundary except for the electrodes. Although different form of the boundary conditions may be used in the forward model, we choose the CEM that takes into account the discrete electrodes, effects of the contact impedance, and the shunting effect of the electrodes.

In addition, the following two constraints for the injected currents and measured voltages are needed to ensure the existence and uniqueness of the solution:

$$\sum_{l=1}^L I_l = 0 \quad (2.5)$$

$$\sum_{l=1}^L U_l = 0 \quad (2.6)$$

The computation of the potential $u(x, y)$ on the Ω and the voltages U_l on the electrodes for the given resistivity distribution $\rho(x, y)$ and boundary conditions is called the forward problem. In general, the forward problem can not be solved analytically we have to resort to the numerical method. There are different numerical methods such as the finite difference method (FDM), boundary element method (BEM), and finite element method (FEM). In this thesis, we used the FEM to obtain the numerical solution.

In the FEM, the object area is discretized into sufficiently small elements having a node at each corner and it is assumed that the resistivity distribution is constant within each element.

Let M be the number of nodes in the finite element mesh. The potential u within the object is approximated as

$$u \approx u^h(x) = \sum_{i=1}^M \alpha_i \phi_i(x) \quad (2.7)$$

and the potential on the electrodes represented as

$$U^h = \sum_{j=1}^{L-1} \beta_j n_j \quad (2.8)$$

where the function ϕ_i is the two-dimensional first order basis function and the bases for the measurements are $n_1 = (1, -1, 0, \dots, 0)^T$, $n_2 = (1, 0, -1, \dots, 0)^T$, $\dots \in \mathfrak{R}^{L \times 1}$ etc. That is, the potentials U_l^h on the electrodes are obtained as

$$U_1^h = \sum_{l=1}^{L-1} \beta_l \quad (2.9)$$

$$\begin{aligned} U_2^h &= -\beta_1 \\ U_3^h &= -\beta_2 \\ &\vdots \\ U_L^h &= -\beta_{L-1} \end{aligned} \quad (2.10)$$

This can be written in the matrix form as

$$U^h = N\beta \quad (2.11)$$

where $N \in \mathfrak{R}^{L \times (L-1)}$ is a sparse matrix such that

$$N = (n_1, n_2, \dots, n_{L-1}) = \begin{bmatrix} 1 & 1 & \dots & 1 \\ -1 & 0 & \dots & 0 \\ 0 & -1 & \dots & 0 \\ \vdots & \vdots & \ddots & \vdots \\ 0 & 0 & \dots & -1 \end{bmatrix} \quad (2.12)$$

This choice for n_j 's ensures that the condition of eq. (2.6) is fulfilled. The linear equation obtained from the finite element formulation $Ab = f$ is constructed such that

$$b = \begin{pmatrix} \alpha \\ \beta \end{pmatrix} \in \mathfrak{R}^{M+L-1} \quad (2.13)$$

$$A = \begin{pmatrix} B & CN \\ (CN)^T & N^T D N \end{pmatrix} \in \mathfrak{R}^{(M+L-1) \times (M+L-1)} \quad (2.14)$$

$$f = \begin{pmatrix} 0 \\ \tilde{\mathbf{I}} \end{pmatrix} = \begin{pmatrix} 0 \\ \sum_{l=1}^L I_l(n_j)_l \end{pmatrix} \in \mathfrak{R}^{M+L-1} \quad (2.15)$$

where $\alpha = (\alpha_1, \alpha_2, \dots, \alpha_M)^T, \beta = (\beta_1, \beta_2, \dots, \beta_{L-1})^T, \tilde{\mathbf{I}} = (I_1 - I_2, I_1 - I_3, \dots, I_1 - I_L)^T \in \mathfrak{R}^{L-1}$ and $0 \in \mathfrak{R}^M$. And the elements of the matrix A (Vauhkonen, 1997) are

$$B(i, j) = \int_{\Omega} \frac{1}{\rho} \nabla \phi_i \nabla \phi_j dx dy + \sum_{l=1}^L \frac{1}{z_l} \int_{e_j} \phi_i \phi_j dS, \quad i, j = 1, 2, \dots, L \quad (2.16)$$

$$C(i, j) = -\frac{1}{z_j} \int_{e_j} \phi_i dS, \quad i = 1, 2, \dots, M, \quad j = 1, 2, \dots, L \quad (2.17)$$

$$D(i, j) = \begin{cases} 0 & i \neq j \\ \frac{|e_i|}{z_j} & i = j \end{cases}, \quad i, j = 1, 2, \dots, L \quad (2.18)$$

where $|e_i|$ is the length of the electrode i .

2.2 Inverse solver for the image reconstruction

The forward problem is to find a unique effect of a given cause by using appropriate physical model. On the contrary, the inverse problems can be interpreted as finding the cause of a given effect or finding the physical law given the cause and effect. These inverse problems do not necessarily have unique and stable solutions and small changes in the data can cause large changes in the solution. Many inverse problems, including EIT, are ill-posed and therefore the problem has to be modified in order to obtain a stable solution. So, the idea of regularization is to replace the ill-posed problem by a nearby well-posed problem.

Image reconstruction in EIT is an inverse problem in which the resistivity distribution of the interior is estimated based on the injected currents and corresponding measured voltages on the boundary of the object.

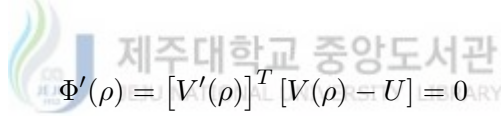
2.2.1 Modified Newton-Rapson method (mNR)

The inverse problem of EIT maps the boundary voltages from experiments to resistivity image. The objective function may be chosen to minimize the error in the least square sense,

$$\Phi(\rho) = \frac{1}{2} [V(\rho) - U]^T [V(\rho) - U] \quad (2.19)$$

where $U \in \mathfrak{R}^{LK \times 1}$ is the vector of measured voltage and $V(\rho) \in \mathfrak{R}^{LK \times 1}$ is the calculated boundary voltage vector that must be matched U .

To find ρ which minimizes the above object function, its derivative is set to zero as:



$$\Phi'(\rho) = [V'(\rho)]^T [V(\rho) - U] = 0 \quad (2.20)$$

where $[V']_{ij} = J_{ij} = \frac{\partial V_i}{\partial \rho_j}$ is the Jacobian matrix. The solution of the above eq. (2.20) uses the Newton-Raphson linearization about a resistivity vector ρ^i at i th iteration as

$$\Phi'(\rho^{i+1}) = \Phi'(\rho^i) + \Phi''(\rho^i)(\rho^{i+1} - \rho^i) = 0 \quad (2.21)$$

The term Φ'' is called the Hessian matrix, expressed as

$$\Phi'' = [V']^T V' + [V'']^T \{I \otimes [V - U]\} \quad (2.22)$$

where \otimes is the Kronecker matrix product. Since V'' is difficult to calculate and relatively small, the second term in the above eq. (2.22) is usually omitted. Therefore the Hessian matrix is modified as

$$\Phi'' = [V']^T V' = J' J = H \quad (2.23)$$

Thus, the iterative equation for updating the resistivity vector based on the above regularized object function is expressed as

$$\rho^{i+1} = \rho^i - H^{-1} \{J^T [V(\rho^i) - U]\} \quad (2.24)$$

where J and H are the Jacobian and the Hessian matrix, respectively.

2.2.2 Modified Newton-Rapson method with Tikhonov regularization

The Hessian matrix is known to be ill-conditioned, which then degrades the performance of the image reconstruction algorithm. To mitigate this problem, the objective function that should be minimized is regularized as:

$$\Phi(\rho) = \frac{1}{2} \{ [V(\rho) - U]^T [V(\rho) - U] + \alpha [R(\rho - \rho^*)]^T [R(\rho - \rho^*)] \} \quad (2.25)$$

where R is the regularization matrix, α is the regularization parameter and ρ^* is the assumed resistivity vector.

Consider first a special case in which $R = I$ and $\rho^* = 0$. This is called the standard Tikhonov regularization method that has been widely used in EIT inverse problems. Consequently, the iterative equation to update the resistivity vector based on the above regularized object function (2.25) is derived as

$$\rho^{i+1} = \rho^i - (H + \alpha I)^{-1} \{J^T [V(\rho^i) - U] + \alpha \rho^i\} \quad (2.26)$$

In more general case in which $R \neq I$, so-called the generalized Tikhonov regularization (Vauhkonen, 1997), the iterative equation to update the resistivity vector based on the above regularized object function (2.25) is derived as

$$\rho^{i+1} = \rho^i - (H + \alpha R^T R)^{-1} \{J^T [V(\rho^i) - U] + \alpha R^T R(\rho^i - \rho^*)\} \quad (2.27)$$

where α is regularization parameter which is chosen *a posteriori*. One popular conventional method for the choice for the regularization matrix R is a difference type matrix on the basis of the generalized Tikhonov regularization technique by the smoothness assumptions in resistivity distributions (Vauhkonen, 1997). In this method, the resistivity distribution is parameterized such that

$$\rho = \sum_{n=1}^N \rho_n X_n \quad (2.28)$$

where X_n is the characteristic function of the n th finite element. The i th row of R is

$$R_i = (0, 0, \dots, 0, -1, 0, \dots, 0, -1, 0, \dots, 0, 3, 0, \dots, 0, -1, 0, \dots, 0) \quad (2.29)$$

where 3 is located at the i th column and -1 is placed in the columns corresponding to elements having common edge with the i th element.

2.2.3 Extended Kalman filter

In case where the resistivity distribution inside the object changes rapidly within the time taken to acquire a full set of independent measurement data, the conventional imaging techniques which need a full set of voltage measurements for each image often fail to obtain satisfactory temporal information on the resistivity distribution. We consider the underlying inverse problem as a state estimation problem to estimate rapidly time-varying distribution of the resistivity. In the state estimation problem, we need so-called the dynamic model which consists of the state equation, i.e., for the temporal evolution of the resistivity and the observation equation, i.e., for the relationship between the resistivity and boundary voltage.

In general, the temporal evolution of the resistivity distribution ρ_k in the object Ω is related by the nonlinear mapping. Here, the state equation is assumed to be of the linear form, of which the modelling uncertainty is compensated by the noise since there is no other information on the temporal evolution of the resistivity distribution in EIT.

$$\rho_{k+1} = F_k \rho_k + w_k \quad (2.30)$$

where $F_k \in \mathfrak{R}^{N \times N}$ is the state transition matrix at time k and N is the number of finite elements in the FEM. In particular, we take $F_k = I_N$ where $I_N \in \mathfrak{R}^{N \times N}$ is an identity matrix, to obtain the so-called *random-walk* model. It is assumed that the process error, w_k is white Gaussian noise with the following covariance which determines the rate of changes in resistivity distribution

$$E[w_k w_k^T] = \Gamma_k^w \quad (2.31)$$

Let $U_k \in \mathfrak{R}^L$, defined as

$$U_k \equiv [U_k^1, U_k^2, \dots, U_k^L]^T \quad (2.32)$$

be the surface measurement voltages induced by the k th current pattern. Then the observation equation can be described as the following nonlinear mapping with measurement error

$$U_k = V_k(\rho_k) + \nu_k \quad (2.33)$$

where the measurement error ν_k is assumed to be white Gaussian noise with covariance

$$E[\nu_k \nu_k^T] = \Gamma_k^\nu \quad (2.34)$$

Linearizing (2.33) about the latest predicted state $\rho_{k|k-1}$ we obtain

$$U_k = V_k(\rho_{k|k-1}) + J_k(\rho_{k|k-1}) \cdot (\rho_k - \rho_{k|k-1}) + H.O.Ts + \nu_k \quad (2.35)$$

where $H.O.Ts$ represents the higher-order terms which will be considered as additional noise, and $J_k(\rho_{k|k-1}) \in \Re^{L \times N}$ is the Jacobian matrix defined by

$$J_k(\rho_{k|k-1}) \equiv \left. \frac{\partial V_k}{\partial \rho} \right|_{\rho=\rho_{k|k-1}} \quad (2.36)$$

Let us define the pseudo-measurement (artificial-measurement) as

$$y_k \equiv U_k - V_k(\rho_{k|k-1}) + J_k(\rho_{k|k-1}) \cdot \rho_{k|k-1} \quad (2.37)$$

Then we obtain the linearized observation equation by considering the $H.O.Ts$ in eq. (2.35) as additional noise

$$y_k = J_k(\rho_{k|k-1}) \cdot \rho_k + \bar{v}_k \quad (2.38)$$

where \bar{v}_k is composed of measurement error and linearization error and also assumed to be white Gaussian noise with covariance as

$$E[\bar{v}_k \bar{v}_k^T] = \Gamma_k \quad (2.39)$$

In Kalman filtering we estimate the state ρ_k based on all the measurements taken up to the time k . With the Gaussian assumptions the required estimate is obtained by minimizing the cost functional which is formulated based on the above state and observation eqs. (2.30) and (2.38), respectively. The cost functional for the conventional Kalman filter is of the form

$$\Xi^a(\rho_k) = \frac{1}{2} \{ \|\rho_k - \rho_{k|k-1}\|_{C_{k|k-1}^{-1}}^2 + \|y_k - J_k(\rho_{k|k-1}) \cdot \rho_k\|_{\Gamma_k^{-1}}^2 \} \quad (2.40)$$

where $C_{k|k-1} \in \Re^{N \times N}$ is the time-updated error covariance matrix, which is defined by

$$C_{k|k-1} \equiv E[(\rho_k - \rho_{k|k-1})(\rho_k - \rho_{k|k-1})^T] \quad (2.41)$$

In order to mitigate the inherent ill-conditioned nature of the EIT inverse problem, additional constraint is included in the cost functional as in eq. (2.40)

$$\Xi^b(\rho_k) = \frac{1}{2} \{ \|\rho_k - \rho_{k|k-1}\|_{C_{k|k-1}^{-1}}^2 + \|y_k - J_k(\rho_{k|k-1}) \cdot \rho_k\|_{\Gamma_k^{-1}}^2 + \alpha \|R\rho_k\|^2 \} \quad (2.42)$$

where α is regularization parameter which is chosen empirically, and R is regularization matrix.

Define the augmented pseudo measurement, $\bar{y}_k \in \Re^{(L+N) \times 1}$ and pseudo-measurement matrix, $H_k \in \Re^{(L+N) \times N}$ as

$$\bar{y}_k \equiv \begin{pmatrix} y_k \\ 0 \end{pmatrix} \quad \text{and} \quad H_k \equiv \begin{pmatrix} J_k \\ \sqrt{\alpha}R \end{pmatrix}, \quad (2.43)$$

respectively. Then the cost functional, eq. (2.42) can be rearranged as

$$\Xi^b(\rho_k) = \frac{1}{2} \{ \|\rho_k - \rho_{k|k-1}\|_{C_{k|k-1}^{-1}}^2 + \|\bar{y}_k - H_k\rho_k\|_{\bar{\Gamma}_k^{-1}}^2 \} \quad (2.44)$$

where the augmented covariance matrix, $\bar{\Gamma}_k \in \Re^{(L+N) \times (L+N)}$ is defined by

$$\bar{\Gamma}_k \equiv \text{Blockdiag}[\Gamma_k, I_N] \quad (2.45)$$

Minimizing the cost functional in eq. (2.44) and solving for the updates of the associated covariance matrices we obtain the recursive extended Kalman filter algorithm (EKF) which consists of the following two steps (Gelb, 1974), (Grewal & Andrews, 1993), (Kim et al, 2001):

(i) Measurement Updating Step (Filtering)

$$G_k = C_{k|k-1} H_k^T [H_k C_{k|k-1} H_k^T + \bar{\Gamma}_k]^{-1} \quad (2.46)$$

$$C_{k|k} = (I - G_k H_k) C_{k|k-1} \quad (2.47)$$

$$\rho_{k|k} = \rho_{k|k-1} + G_k [\bar{y}_k - H_k \rho_{k|k-1}] \quad (2.48)$$

(ii) Time Updating Step (Prediction)

$$C_{k+1|k} = F_k C_{k|k} F_k^T + \Gamma_k^w \quad (2.49)$$

$$\rho_{k+1|k} = F_k \rho_{k|k} \quad (2.50)$$

Hence, we can find the estimated state $\rho_{k|k}$ for the true state ρ_k in a recursive minimum mean square error sense for $k = 1, 2, \dots, rK$, where K is the number of the independent current patterns and r is the number of the classical frames.

2.2.4 Calculation of Jacobian

The Jacobian matrix

$$J = \begin{bmatrix} \frac{\partial U^{(1)}}{\partial \rho_1} & \dots & \frac{\partial U^{(1)}}{\partial \rho_N} \\ \vdots & \dots & \vdots \\ \frac{\partial U^{(K)}}{\partial \rho_1} & \dots & \frac{\partial U^{(K)}}{\partial \rho_N} \end{bmatrix} \quad (2.51)$$

where $U^{(K)} \in \mathfrak{R}^L$ is the vector induced by k th current pattern, can be computed by the standard method (Vauhkonen, 1997).

From the finite element formulation $Ab = f$, the n 'th column of the Jacobian J can be obtained from

$$\frac{\partial b}{\partial \rho_n} = \frac{\partial (A^{-1}f)}{\partial \rho_n} = -A^{-1} \frac{\partial A}{\partial \rho_n} A^{-1}f = -A^{-1} \frac{\partial A}{\partial \rho_n} b \quad (2.52)$$

in which $\frac{\partial A(m,i)}{\partial \rho_n} = -\frac{1}{\rho_n^2} \int_{\Delta_n} \nabla \phi_m \nabla \phi_i dx dy$. Here, Δ_n is the element with respect to which the derivative is calculated.

In the FEM discretization, the $L - 1$ last lows of $\frac{\partial b}{\partial \rho_n}$ correspond to the derivatives of the electrode voltages from which the derivative $\frac{\partial U^{(k)}}{\partial \rho_n}$ can be computed by using eq. (2.9) ~ (2.11).



III. Dynamical electrical impedance tomography with prior information

In the previous chapter, dynamic imaging techniques have been developed to enhance the temporal resolution of the reconstructed images in the situations where the resistivity distribution inside the object changes rapidly in time. In most of these techniques, the inverse reconstruction problem is treated as state estimation problem and the time-varying state is estimated with the aid of LKF or EKF.

In real situations there are partially known fixed internal structures and/or resistivities inside the object. These internal structures can be, for example, an impeller drive shaft or a mixing paddle in process vessels and an assembly of fuel rods in nuclear reactor. The internal structures inside the object may result in difficulties in the image reconstruction in EIT especially in the case where the high resistive region is near the conductive internal structure. The so-called masking effect in the reconstructed image may be significant for the high-contrast case. There are two ways to get around these difficulties; the one is to use the internal structure as additional electrodes and the other is to take into account it as *a priori* information in the inverse procedure (Heikkinen et al, 2001). That is the available *prior* information can be included into the dynamic image reconstruction algorithm. If we have some *prior* knowledge on the location and possibly the resistivity of the structure, it would be desirable to implement it into the inverse problem. The location of the internal structure can be included in the mesh that is used in the image reconstruction and the edges of the structure as well as the resistivity value can be considered in the regularization of the solution.

We proposed to develop a dynamic EIT reconstruction algorithm for the case where the fixed internal structure and/or its resistivity are known partially and the resistivity distribution of the other part inside the object changes rapidly within the time taken to acquire a full set of independent measurement data. To achieve the purpose, in section 3.1 we propose method EKF-SR, an additional constraint for the

known internal structure and/or its resistivity is incorporated into the cost functional as *a priori* information. In section 3.2, we propose method EKF-IE. This method is to use the internal known structure as additional electrodes.

The proposed inverse problems are treated as the state estimation problem and the unknown state (resistivity) is estimated with the aid of the EKF in a minimum mean square error sense. In other to deal with the well known ill-posedness of the EIT inverse problem, smoothness assumption is made and the modified Tikhonov regularization technique is also introduced in the cost functional. In doing so, we can enhance the temporal and spatial resolution for the reconstructed image.

3.1 Partially known internal structure & resistivity (EKF-SR)

Sometimes in real situations, there are partially known internal structures and/or its resistivities. These additional information inside the object can be taken into account as *a priori* information in the cost functional as

$$\begin{aligned} \Xi(\rho_k) = \frac{1}{2} \{ & \|\rho_k - \rho_{k|k-1}\|_{C_{k|k-1}^{-1}}^2 + \|y_k - J_k(\rho_{k|k-1}) \cdot \rho_k\|_{\Gamma_k^{-1}}^2 \\ & + \alpha \|R^* \rho_k\|^2 + \beta \|L(\rho_k - \rho^*)\|^2 \} \end{aligned} \quad (3.1)$$

where R^* is obtained from R by removing the -1 in eq. (2.29) that corresponds to element having common edge with the known internal structure. In that case, the number 3 in eq. (2.29) is also replaced by 2 since the smoothness assumption is violated between the known element and background. The norm in the last two terms in eq. (3.1) is the common 2-norm without any weighting factor. In eq. (3.1), the sparse matrix L is constructed to pick out the elements corresponding to the known structure. If we know the location and resistivities of P elements inside the object, $\rho^* \in \mathfrak{R}^N$ is constructed such that it contains resistivity of P elements corresponding to the known structure and zeros of $N - P$ elements and the dimension of the extraction matrix is $L \in \mathfrak{R}^{P \times N}$. The i th row of the extraction matrix, L_i is constructed such that it contains zeros for $(N - 1)$ elements and only one 1 at the j th column if the resistivity of the j th element is assumed to be known. In addition, β is another weighting factor representing the confidence on the assumed resistivity

of the internal known structure. The value of β can be chosen to be large if the resistivities of the internal structure are known accurately. If we know the location of the internal structure but not the resistivity, the value of β is equal to zero.

Define the augmented pseudo-measurement, $Y_k \in \mathfrak{R}^{(L+N+P) \times 1}$ and pseudo measurement matrix, $\overline{H}_k \in \mathfrak{R}^{(L+N+P) \times N}$ as

$$Y_k \equiv \begin{pmatrix} y_k \\ 0 \\ \sqrt{\beta}L\rho^* \end{pmatrix} \quad \text{and} \quad \overline{H}_k \equiv \begin{pmatrix} J_k \\ \sqrt{\alpha}R^* \\ \sqrt{\beta}L \end{pmatrix} \quad (3.2)$$

Then the cost functional (3.1) can be rearranged as

$$\Xi(\rho_k) = \frac{1}{2} \{ \|\rho_k - \rho_{k|k-1}\|_{C_{k|k-1}}^2 + \|Y_k - \overline{H}_k \rho_k\|_{\Gamma}^2 \} \quad (3.3)$$

where the augmented covariance matrix, $\Gamma \in \mathfrak{R}^{(L+N+P) \times (L+N+P)}$ is defined by

$$\Gamma \equiv \text{Blockdiag}[\Gamma_k, I_N, I_P] \quad (3.4)$$

Minimizing the cost functional in eq. (3.3) and solving for the updates of the associated covariance matrices we obtain the recursive extended Kalman filter algorithm which consists of the following two steps:

(i) Measurement Updating Step (Filtering)

$$G_k = C_{k|k-1} \overline{H}_k^T [\overline{H}_k C_{k|k-1} \overline{H}_k^T + \Gamma]^{-1} \quad (3.5)$$

$$C_{k|k} = (I - G_k \overline{H}_k) C_{k|k-1} \quad (3.6)$$

$$\rho_{k|k} = \rho_{k|k-1} + G_k [Y_k - \overline{H}_k \rho_{k|k-1}] \quad (3.7)$$

(ii) Time Updating Step (Prediction)

$$C_{k+1|k} = F_k C_{k|k} F_k^T + \Gamma_k^w \quad (3.8)$$

$$\rho_{k+1|k} = F_k \rho_{k|k} \quad (3.9)$$

As a result, the only difference between the conventional EKF and the proposed EKF-SR which includes *a priori* information for the partially known internal structure is that the dimension of the measurement updating procedure is increased.

3.2 Internal electrode attached to the known internal structure (EKF-IE)

The sensitivity of EIT depends on the current density inside the object. In the areas where the current density is low the resistivity changes may not cause detectable changes on the measured voltages on the electrodes. In conventional EIT one uses only the electrodes attached on the surface of the object. Thus, the current density in the center of the object is quite low and the sensitivity is poor.

In some cases, there are *prior* known internal structures of the object that could be used as internal electrodes. By injecting currents through the internal electrode the current density and the sensitivity can be increased.

The purpose of this section is to develop a dynamic EIT reconstruction method for the case where the fixed internal structure which used as internal electrodes. The inverse problem is treated as the state estimation problem and the unknown state (resistivity) is estimated with the aid of the EKF consists of the above eqs. (2.46)~(2.50). In order to deal with the well-known ill-posedness of the EIT inverse problem, smoothness assumption is made and the modified Tikhonov regularization technique is also introduced in the cost functional as R^* in section 3.1. That is, R_i in eq. (2.29) that corresponds to element of the internal electrode is replaced as

$$R_i^* = (0, 0, \dots, 0, -1, 0, \dots, 0, 0, 0, \dots, 0, 2, 0, \dots, 0, -1, 0, \dots, 0) \quad (3.10)$$

IV. Computer simulations & experimental results

4.1 Partially known internal structure & resistivity

We carried out both the computer simulations with synthetic data and experiments with real measurement data to evaluate the reconstruction performance of the proposed algorithm. In both cases, the complete electrode model with 32 electrodes(L) and trigonometric current patterns with two classical frames(r) were employed. For convenience, we assumed that the structure and/or its resistivity located at center of the object are known *a priori*. The trigonometric current patterns for one classical frame are of the form

$$\begin{aligned} I_k(l) &= M_k \cos(k\zeta_l), \quad l = 1, 2, \dots, L, k = 1, 2, \dots, \frac{L}{2} \\ &= M_k \sin((k - \frac{L}{2})\zeta_l), \quad l = 1, 2, \dots, L, k = \frac{L}{2} + 1, \dots, L - 1 \end{aligned} \quad (4.1)$$

where $\zeta_l = 2\pi l/L$ and the amplitude of the injected current M_k is set to 1 for all k .

The FEM meshes used for the forward and inverse solvers are shown in Fig. 4.1 (a) and (b), respectively. In the forward computations we used the FEM with a mesh of 3104 elements and 1681 nodes(M). In the inverse computations, we used the FEM with a mesh of 776 elements(N) and 453 nodes to reduce the computational burden and mitigate the ill-posed characteristics of the inverse problem.

To compare the reconstruction performance, we used the modified Newton-Raphson algorithm with partially known internal structure and resistivities (mNR-SR) (Heikkinen et al, 2001), dynamic algorithm with the extended Kalman filter (EKF) (Kim et al, 2001), and the extended Kalman filter with partially known internal structure and resistivities (EKF-SR) which is described in this thesis. The parameters used for the three methods are as follows. The regularization parameter(α) is set to 0.1 and 1.0 in the simulation and experiment, respectively. The weighting factor(β) for *a priori* information in EKF-SR is set to 1.0 and 10.0 in the simulation and experiment, respectively. The initial resistivity value is set to the same as

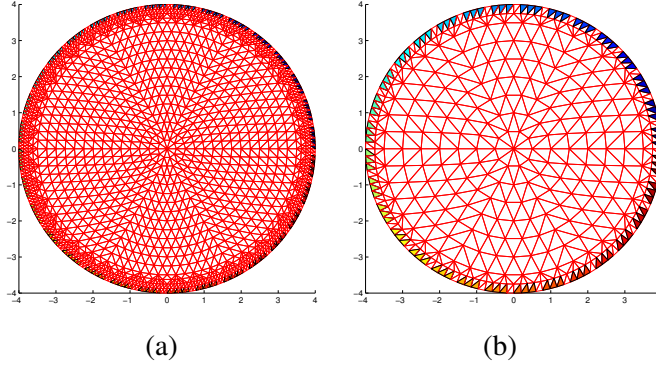


Fig. 4.1. FEM meshes for (a) forward solver and (b) inverse solver.

the background value in all cases. For simplicity, it is assumed that the covariance matrices for all the EKFs are diagonal and time-invariant. The covariance matrix for process noise(Γ_k^w) is $10I_N$ and $0.1I_N$ in the simulation and experiment, respectively. The covariance matrix for measurement noise(Γ_k) is $10^{-6}I_L$ and $10^{-2}I_L$ in the simulation and experiment, respectively. The initial value for the state error covariance matrix($C_{1|0}$) is I_N in both cases.

4.1.1 Computer simulation results

We generated the following sequence of resistivity distributions to simulate a dynamic situation. We assumed that there is known conductive circular structure ($2cm$ in diameter, resistivity of $10\Omega cm$) located at the center of the domain. An almost circular-type target (resistivity of $600\Omega cm$) was moved abruptly to the opposite site through near the center after 16 current patterns in a circular domain ($8cm$ in diameter, $300\Omega cm$ background resistivity) as depicted in the first column of Fig. 4.2.

Fig. 4.2 shows the reconstructed images for the three methods in which the color-bar represents resistivity value. The images in the second column are reconstructed by the EKF. As can be seen clearly, the location (temporal resolution) of the moving target is rather misleading especially when the target is located near the conductive center of the domain (2nd and 3rd rows in the 2nd column). It seems that the error may be generated from the masking effect for the high-contrast ratio (in this case the contrast ratio is $60 : 1$). Also, the background was severely blurred by the conductive circular structure. The third column represents the reconstructed

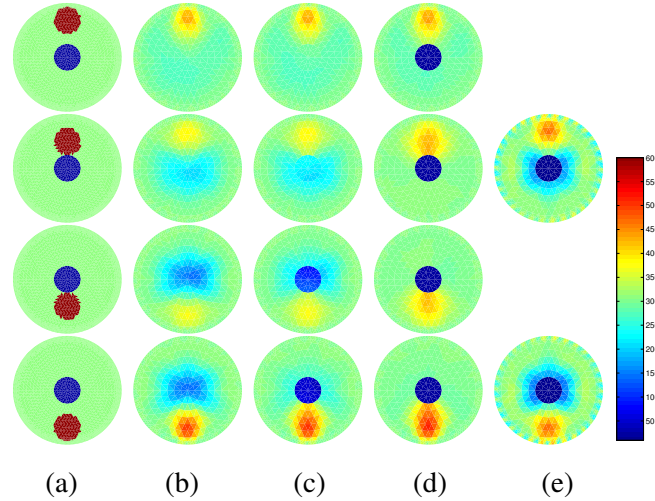


Fig. 4.2. Reconstructed images from the computer simulation. (a) True images, (b) reconstructed images by the EKF, (c) reconstructed images by the EKF-SR when $\beta = 0$, (d) reconstructed images by the EKF-SR when $\beta = 1$, and (e) reconstructed images by the mNR-SR.

images from the EKF-SR when $\beta = 0$. This case means that we know only the location of internal structure. The images obtained for the first frame (1st and 2nd rows in the 3rd column) are similar to those of the EKF. However, the images obtained for the second frame (3rd and 4th rows in the 3rd column) are more clear than those of the EKF. The fourth column represents the reconstructed images from the EKF-SR when $\beta = 1$. As can be expected, the reconstruction performance is improved qualitatively in terms of the temporal and spatial resolution. The reconstructed images obtained from the mNR-SR (5th column) are also blurred and the information on the time-variability of the moving target is lost since it requires a full set of measurement data.

4.1.2 Experimental results

We have developed an EIT measurement system (Fig. 4.3) that consists of a pentium PC, data acquisition board and control software, current generator and switching board, and a cylindrical phantom with 32 electrodes that cover approximately 55% of the inner circumference. The phantom simulates a two-dimensional situation.



Fig. 4.3. EIT measurement system

The cylindrical phantom (8cm in diameter) was filled up with saline ($NaCl$) having resistivity of approximately $330\Omega cm$. We placed cylindrical iron rod (1.3cm in diameter, resistivity of $0.5\Omega cm$) at the center of the phantom and one or two cylindrical plastic target (2cm in diameter) was moved abruptly after every 16 current patterns (1st column of Fig. 4.4) to simulate more complex dynamic system with partially known internal structure.

Fig. 4.4 (b), (c), (d), and (e) shows the reconstructed images obtained by the EKF, EKF-SR when $\beta = 0$, EKF-SR when $\beta = 10$, and mNR-SR, respectively. As can be seen in these Figs, the reconstructed images from the EKF and EKF-SR when $\beta = 0$ for the moving targets near the center are obscure while those from the EKF-SR when $\beta = 10$ are more visible. As in the simulation results, it is also pointed that the employed *a priori* information located at the center has a significant effect on the reconstruction performance of the moving targets located near the center.

Compared to the simulations the reconstruction performance is worse with real measurements. For example, the truly homogeneous background is more nonhomogeneous in the experiment than in the simulation and also the moving target is not as clearly discerned. These artifacts can be due to the random noise in the measurements but this does not explain a systematic artifact that can be seen in the center of the tank, near the rod. Possible explanations for this are that the rod was bigger (1.3cm in diameter) in the experiment than it was assumed to be (1.0cm), when the reconstruction was carried out.

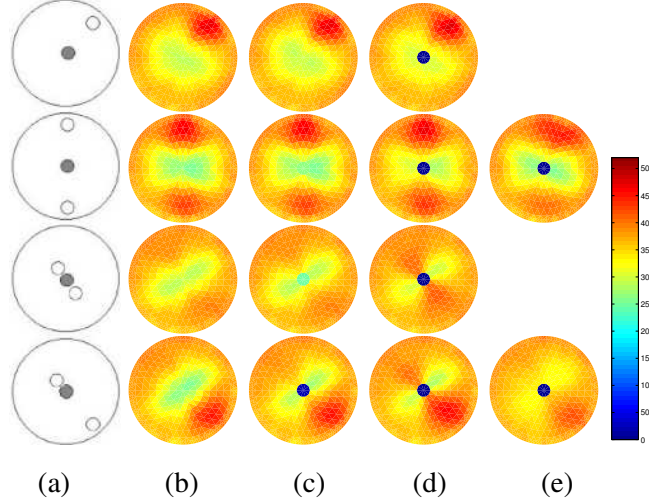


Fig. 4.4. Reconstructed images from the experiment. (a) True images, (b) reconstructed images by the EKF, (c) reconstructed images by the EKF-SR when $\beta = 0$, (d) reconstructed images by the EKF-SR when $\beta = 10$, and (e) reconstructed images by the mNR-SR.

4.1.3 Errors in the reconstructions

We also computed errors in the reconstructions for EKF and for the EKF-SR with $\beta = 0$ and $\beta = 1$. The error (*RMSE*) for each current pattern k was computed as

$$RMSE(k) = \sqrt{\frac{(\rho_k - \rho_{k|k})^T (\rho_k - \rho_{k|k})}{\rho_k^T \rho_k}} \quad (4.2)$$

where ρ_k and $\rho_{k|k}$ are the true resistivity distribution and the estimated resistivity distribution at the k th current pattern, respectively. The result is shown in Fig. 4.5.

As it can be seen from Fig. 4.5, the error in the image reconstruction is dramatically reduced in the simulation, when the internal structure is considered in the reconstruction procedure.

4.1.4 Effects of parameter values (α, β) on the reconstruction performance

In order to investigate how the parameters α and β affect the image reconstruction, we choose the simulation (Fig. 4.2) and made the EKF-SR reconstructions with different choices for α and β .

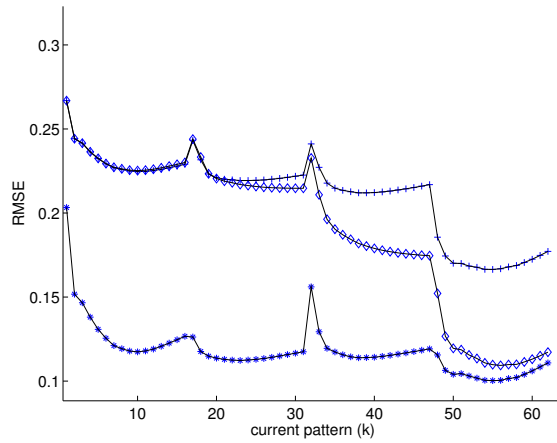


Fig. 4.5. Reconstruction errors RMSE for the simulation. (+) is for EKF, (\diamond) for EKF-SR with $\beta = 0$ and (*) for EKF-SR with $\beta = 1$.

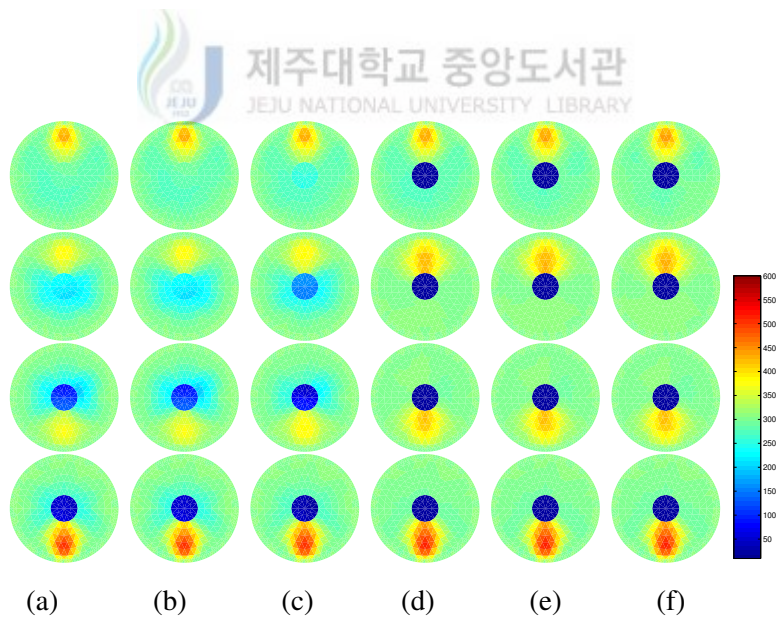


Fig. 4.6. Reconstructed images (in Ω_{cm}) from the variable β tests. The parameter α was fixed to 0.1. Reconstruction with (a) $\beta = 0$, (b) $\beta = 10^{-4}$, (c) $\beta = 10^{-2}$, (d) $\beta = 0.2$, (e) $\beta = 1$, and (f) $\beta = 10$.

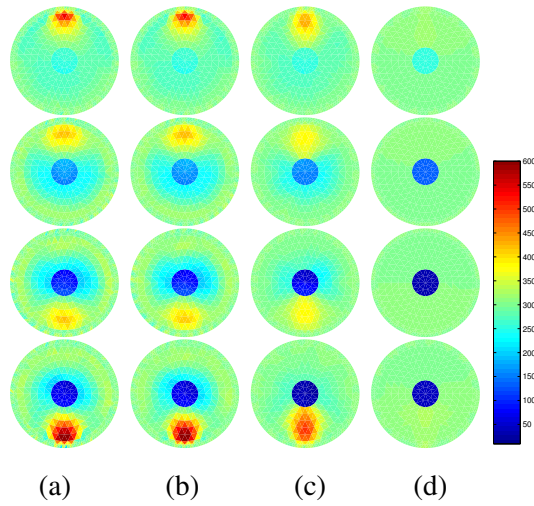


Fig. 4.7. Reconstructed images (in Ωcm) from the variable α tests. The parameter β was fixed to 0.01. Reconstruction with (a) $\alpha = 10^{-4}$, (b) $\alpha = 10^{-2}$, (c) $\alpha = 0.1$, and (d) $\alpha = 1$.

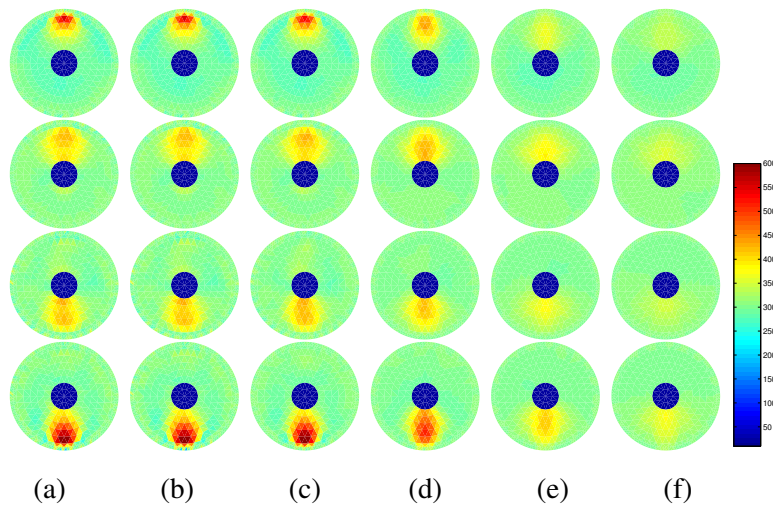


Fig. 4.8. Reconstructed images (in Ωcm) from the variable α tests. The parameter β was fixed to 1. Reconstruction with (a) $\alpha = 10^{-6}$, (b) $\alpha = 10^{-3}$, (c) $\alpha = 10^{-2}$, (d) $\alpha = 0.1$, (e) $\alpha = 0.3$, and (f) $\alpha = 0.5$.

In Fig. 4.6, we fixed the α value to 0.1 and changed the β value from 0 to 10. As we can see in eq. (3.1) in the manuscript, β is weighting factor for the assumed resistivity of the internal structure. If we give a large value for β this means that we strongly believe that the resistivity of the internal structure is ρ^* . As can be expected, we increase the value of β we see more enhanced reconstruction performance for the known internal structure since the resistivity is forced to be close to the given ρ^* .

The regularization parameter α includes two types of information when connected to R^* . Firstly, as we increase α we get smooth results almost everywhere, except on the boundary of the internal structure. Secondly, the internal structure becomes more pronounced as we increase α since the regularization includes the information on the jump between the structure and the background.

This effect can be seen in the Figs. 4.7 and 4.8. Large value for α gives very sharp image of the internal structure, diminishing the image of the target at the same time. Too large value for α lost the target completely due to the smoothness assumption. In addition, as shown in Fig. 4.8 with $\beta = 1$, if β is large enough, α is not needed for making the internal structure distinct.

4.2 Internal electrode attached to the known internal structure

We carried out extensive computer simulations with synthetic data to evaluate the reconstruction performance of the proposed algorithm.

The FEM meshes without internal electrode used for the forward and inverse solvers are shown in Fig. 4.9 (a) and (b), respectively. In the forward computations we used the FEM with a mesh of 2400 elements and 1281 nodes. In the inverse computations, we used the FEM with a mesh of 600 elements and 341 nodes. For the current injection and corresponding voltage measurement, traditional adjacent method (Webster, 1990) was employed through 16 boundary electrodes (L) so that the total measurement voltage data were $256(16 \times 16)$.

The FEM meshes with a single internal electrode used for the forward and inverse solvers are shown in Fig. 4.10 (a) and (b), respectively. In the forward computations we used the FEM with a mesh of 2480 elements and 1336 nodes. In the

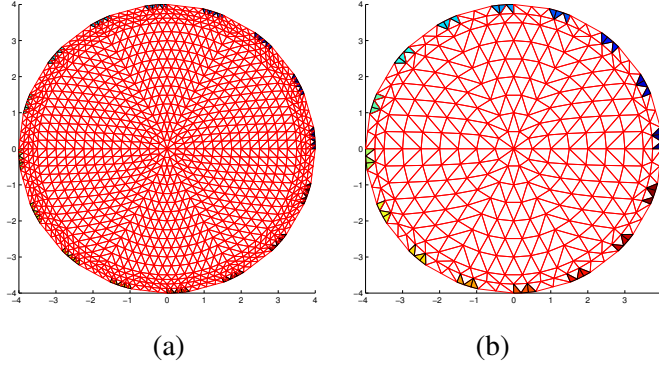


Fig. 4.9. FEM meshes without internal electrode used for (a) forward solver and (b) inverse solver.

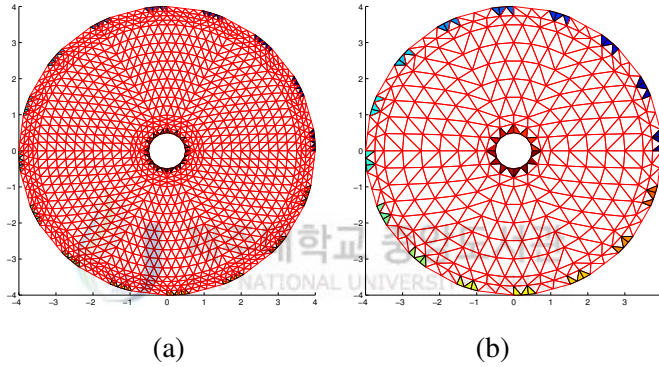


Fig. 4.10. FEM meshes with an internal electrode used for (a) forward solver and (b) inverse solver.

inverse computations, we used the FEM with a mesh of 620 elements and 358 nodes. We injected electrical current between 16 boundary electrodes and the internal electrode and measured the corresponding voltage on the 17 electrodes (L) so that the total measurement voltage data were $272(17 \times 16)$.

To compare the reconstruction performance, we used the static algorithm based on the modified Newton-Raphson algorithm with internal electrode (mNR-IE) (Heikkinen et al, 2001), dynamic algorithm based on the extended Kalman filter (EKF) (Kim et al, 2001), and the extended Kalman filter with internal electrode (EKF-IE) described in this thesis. The parameters used for the three methods are as follows. The regularization parameter (α) is set to 0.5 in both simulations. The initial resistivity value is set to the same as the background value in all cases. For simplicity,

it is assumed that the covariance matrices for all the EKFs are diagonal and time-invariant. The covariance matrix for process noise (Γ_k^w) is $10I_N$, the covariance matrix for measurement noise (Γ_k) is $0.0001I_N$ and the initial value for the state error covariance matrix ($C_{1|0}$) is I_N in both simulations.

4.2.1 The first simulation results

For the verification of the proposed model, we simulate in a circular domain ($8cm$ in diameter). It is assumed that there is a known conductive circular structure (about $1cm$ in diameter, $0.0001\Omega cm$ in resistivity), which is located at the center and is used as an internal electrode.

We generated the following sequence of resistivity distributions to simulate a dynamic situation. We assume a single anomaly emerges and disappears, and then, three anomalies emerge and disappear. The background resistivity and the anomaly resistivity are set to $300\Omega cm$ and $600\Omega cm$, respectively. The simulated evolution of the resistivity distribution is depicted in Fig. 4.11 (a). Each transient interval is equivalent to 4 current injections. Also, In order to make the simulation more realistic, we assume that the measured boundary voltages are contaminated by the measurement error of 1%.

Fig. 4.11 shows the reconstructed images for the three methods. The images in Fig. 4.11(b) are reconstructed by the EKF without internal electrode. As can be seen clearly, the location (temporal resolution) of the moving target is rather misleading. It seems that the error may be generated from the masking effect for the high-contrast. The Fig. 4.11(c) represents the reconstructed images from the EKF-IE. As can be expected, the reconstruction performance is improved qualitatively in terms of the temporal and spatial resolution. The reconstructed images in Fig. 4.11(d) obtained from the mNR-IE are also vague and the information on the time-variability of the moving target is lost since it requires a full set of measurement data.

4.2.2 The second simulation results

In the second simulation, we assume the same condition for the internal structure and the resistivity values as in the first simulation. In the measurement of boundary voltages, as in the first simulation, random error of 1% is included. However, a

different evolution of mixture distribution is considered as shown in Fig. 4.12(a).

As much similar to the results from the first simulation, mNR-IE cannot extract any useful information from the EIT image reconstruction. Even with EKF, the reconstruction seems to be more deteriorated compared to the first simulation. It should be noted that in this simulation we intentionally place two anomalies and the conductive internal structure close together. Then, resistive anomalies impede electrical current flowing to the conductive internal structure and the spatial resolution is expected to substantially worsen. However, the utilization of the internal electrode improves the spatial resolution in Fig. 4.12(c).

4.2.3 Effects of parameter value (α) on the reconstruction performance

To investigate how the regularization parameter affects the image reconstruction, we made EKF-IE reconstructions for the same scenario as the first simulation with different choices for α . The results are shown in Fig. 4.13. As we can see from eq. (2.42), α is the weighting factor for the Tikhonov regularization. As we increase the value of α from 5×10^{-6} to 5 we get very homogeneous background images, but diminishing the sharpness for the moving target at the same time. Generally speaking, too small a value for α results in continued instability of the solution, whereas too large a value results in an overregularized solution that, while stable, has an unnecessarily large reconstruction error.

4.2.4 Effects of the measurement and linearization error on the reconstruction performance

In order to see how the uncertainty $\bar{\nu}_k$ in the measurement eq. (2.38) affects the image reconstruction, we chose the first simulation and made the EKF-IE reconstructions with different choices for the noise level. As can be seen from the Fig. 4.14, the reconstruction performance of the EKF-IE deteriorates if we increase the level of the noise. As can be expected, too high level of the uncertainty lost the targets completely as in the last column of the Fig. 4.14.

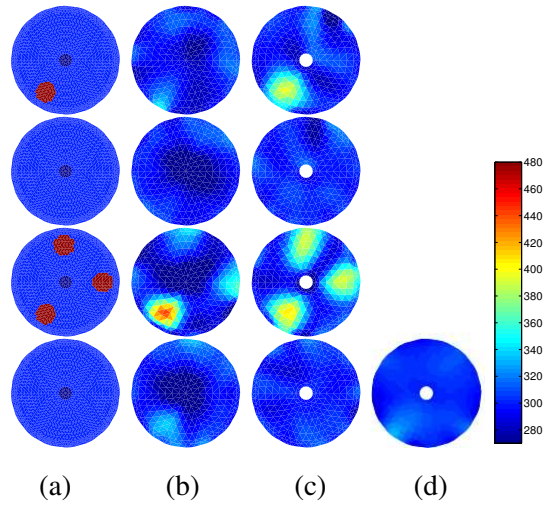


Fig. 4.11. Reconstructed images for the first simulation. (a) True images, (b) reconstructions with EKF, (c) reconstructions with EKF-IE, and (d) reconstructions with mNR-IE.

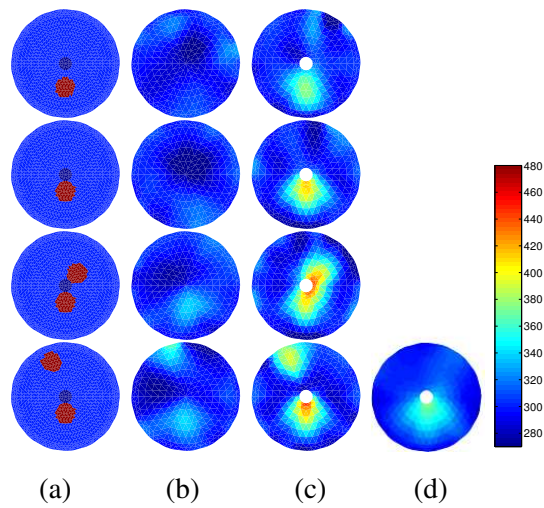


Fig. 4.12. Reconstructed images for the second simulation. (a) True images, (b) reconstructions with EKF, (c) reconstructions with EKF-IE, and (d) reconstructions with mNR-IE.

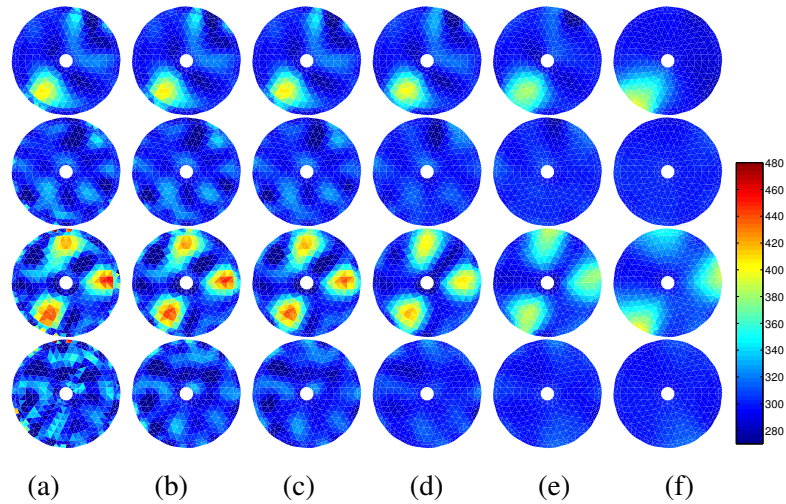


Fig. 4.13. Reconstructed images for the first simulation with different values of α . Reconstruction with (a) $\alpha = 5 \times 10^{-6}$, (b) $\alpha = 0.05$, (c) $\alpha = 0.3$, (d) $\alpha = 0.5$, (e) $\alpha = 1$, and (f) $\alpha = 5$.

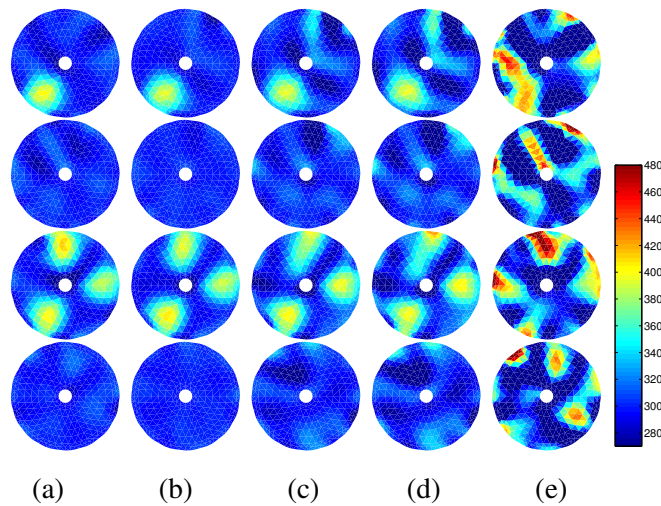


Fig. 4.14. Reconstructed images for the first simulation with different noise levels. Reconstruction with (a) free noise, (b) 0.5% noise, (c) 2.0% noise, (d) 3.0% noise, and (e) 9.0% noise.

V. Conclusions

In usual static EIT techniques, the internal resistivity distribution is assumed to be stationary during the measurement of the required full set of independent EIT data.

Quite often in real situations, however, the object to be visualized may undergo severe transient. The situation considered in this thesis is the application of the EIT technique to the visualization of resistivity distribution under rapid transient within the time taken to acquire a full set of independent measurement data. In addition, there are partially known fixed internal structures and resistivity inside the object.

For the dynamic electrical impedance imaging with *prior* information, EIT inverse problem is formulated as a state estimation problem and the state (resistivity distribution) is estimated with the aid of EKF after the voltage measurements corresponding to each current pattern. Additional information for the known internal structure and its resistivity is incorporated in the cost functional as *prior* information so that the measurement updating procedure in the EKF is modified slightly (EKF-SR). In addition, internal electrode is attached to the internal structure in addition to the external electrodes to improve the spatial resolution of the reconstruction image.

The reconstruction performance of the proposed dynamic reconstruction algorithms (EKF-SR and EKF-IE) was compared with that of the existing algorithms through computer simulations and laboratory experiments. The results show that the proposed methods improve reconstruction performance significantly in the sense of the spatial and temporal resolution.

Of course, there are many alternatives to the extended Kalman filter used in this thesis. For example, LKF can be replaced by the EKF to reduce the on-line computational burden. Further research will be carried out to test the reconstruction performance of the proposed technique for more complicated real situations.

Summary

Electrical impedance tomography (EIT) is a relatively new imaging modality in which the internal impedivity distribution is reconstructed based on the known sets of injected currents and measured voltages on the an array of electrodes which are attached on the boundary of an object.

In this thesis, dynamic EIT imaging techniques are described for the case where the fixed internal structure and/or its resistivity are known partially and the resistivity distribution of the other part inside the object changes rapidly within the time taken to acquire a full set of independent measurement data. Two methods are proposed to enhance reconstruction performance in EIT, in which available *prior* information is exploited. In the first method, an additional constraint for the known internal structure and/or its resistivity is incorporated into the cost functional as *a priori* information and in the second method the internal electrode is attached to the internal structure in addition to the external electrodes. The inverse problem is treated as the state estimation problem and the unknown state (resistivity) is estimated with the aid of the extended Kalman filter in a minimum mean square error sense. In other to deal with the well known ill-posedness of the EIT inverse problem, smoothness assumption is made and the modified Tikhonov regularization technique is also employed in the cost functional.

To illustrate the reconstruction performance of the proposed algorithm, we carried out extensive computer simulations for synthetic and experimental data. The results show that the proposed algorithm has enhanced reconstruction performance than that of the existing methods in the sense of temporal and spatial resolution.

References

- Barber D. C. and Brown B. H., 1984, "Applied potential tomography," *Journal of Physics E: Scientific Instrumentation*, Vol. 17, pp. 723-733.
- Beck M. S. and Williams R. A., 1996, "Process tomography : a European innovation and its applications," *Measurement Science and Technology*, Vol. 7, pp. 215-224.
- Ceccio S. L. and George D. L., 1996, "Review of electrical impedance techniques for the measurement of multiphase flows," *Journal of Fluids Engineering*, Vol. 118, pp. 391-399.
- Cheney M., Isaacson D., and Newell J. C., 1999, "Electrical impedance tomography," *SIAM Review*, Vol. 41, No. 1, pp. 85-101.
- Cheng K.-S., Isaacson D., Newell J.C., and Gisser D.G., 1989, "Electrode Models for electric current computed tomography," *IEEE Transactions on Biomedical Engineering*, Vol. 36, pp. 918-924.
- Dickin F. and Wang M., 1996, "Electrical resistance tomography for process tomography," *Measurement Science Technology*, Vol. 7, pp. 247-260.
- Gelb A., 1974, *Applied Optimal Estimation*, The M. I. T. Press, Cambridge, Massachusetts.
- Grewal M. S. and Andrews A. P., 1993, *Kalman Filtering : Theory and Practice*, Prentice Hall, Englewood Cliffs, New Jersey.
- Heikkinen L. M., Vauhkonen M., Savolainen T., Leinonen K., and Kaipio J. P., 2001, "Electrical Process Tomography with known internal structures and resistivities," *Inverse Problems in Engineering*, Vol. 9, pp. 431-454.
- Heikkinen L. M., Vauhkonen M., Savolainen T., and Kaipio J. P., 2001, "Modelling of internal structures and electrodes in electrical process tomography," *Measurement Science and Technology*, Vol. 12, pp. 1012-1019.
- Kaipio J. P., Karjalainen P. A., Somersalo E., and Vauhkonen M., 1999, "State estimation in time-varying electrical impedance tomography," *Annals of New York Academy of Sciences*, Vol. 873, pp. 430-439.
- Kang S. I. and Kim K. Y., 2001, "Dynamic Electrical Impedance Tomography with

- Internal Electrodes”, *Journal of IKEEE*, Vol. 5, No. 2, pp. 33-43.
- Kim K. Y., Kim B. S., Kim M. C., Lee Y. J., and Vauhkonen M., 2001, “Image reconstruction in time-varying electrical impedance tomography based on the extended Kalman filter,” *Measurement Science and Technology*, Vol. 12, pp. 1032-1039.
- Kim K. Y., Kim B. S., Kim M. C., and Lee Y. J., 2001, “On-line image reconstruction in dynamic electrical impedance tomography based on the extended Kalman filter,” *Proc. Of Compumag-Evian, France*, Vol. 4, pp. 70-71.
- Kim K. Y., Kang S. I., Kim M. C., Kim S., Lee Y. J. and Vauhkonen M., 2002, “Dynamic Image Reconstruction in Electrical Impedance Tomography with Known Internal Structures,” *IEEE Transaction on Magnetics*, Vol. 38, No. 2, pp. 1301-1304.
- Kim K. Y., Kang S. I., Kim M. C., Kim S., Lee Y. J. and Vauhkonen M., in press, “Dynamic Electrical Impedance Tomography with Known Internal Structures,” *Inverse Problem in Engineering*.
- Kim K. Y., Kang S. I., Kim M. C., Lee J. H., Kim S., and Kang C. I., 2002, “Dynamic Electrical Impedance Imaging of Binary-Mixture Fields with External And Internal Electrodes,” *4th International Conference on Inverse Problem in Engineering*, Rio de Janeiro, Brazil.
- Peyton A. J., Yu Z. Z., Lyon G., Al-Zeibak S., Ferreira J., Velez J., Linhares F., Borges A. R., Xiong H. L., Saunders N. H., and Beck M. S., 1996, “An overview of electromagnetic inductance tomography : description of three different systems,” *Measurement Science Technology*, Vol. 7, pp. 261-271.
- Seppanen A., Vauhkonen M., Vauhkonen P. J., Somersalo E., and Kaipio J. P., 2001, “State estimation with fluid dynamical evolution models in process tomography-EIT applications,” *Inverse Problems*, Vol. 17, pp. 467-484.
- Smith R. W. M., Freeston I. L., and Brown B. H., 1995, “A real-time electrical impedance tomography system for clinical use-Design and preliminary results,” *IEEE Transactions on Biomedical Engineering*, Vol. 42, No.2, pp. 133-140.
- Vauhkonen M., Karjalainen P. A., and Kaipio J. P., 1998, “A Kalman filter approach to track fast impedance changes in electrical impedance tomography,” *IEEE Transactions on Biomedical Engineering*, Vol.45, No.4, pp. 486-493.

- Vauhkonen M., 1997, Electrical Impedance Tomography and Prior Information, Doctoral Dissertation, Dept. of Applied Physics, University Kuopio.
- Vauhkonen, P. J., Vauhkonen M., Makinen T., Karjalainen P. A. Karjalainen, and Kaipio J. P., 2000, "Dynamic electrical impedance tomography - Phantom studies," *Inverse Problems in Engineering*, Vol. 8, pp. 495-510.
- Vauhkonen M., Lionheart W.R.B., Heikkinen L.M., Vauhkonen P.J., and Kaipio J.P., 2001, "A MATLAB package for the EIDORS Project to reconstruct two-dimensional EIT images," *Physiological Measurements*, Vol. 22, pp. 107-111.
- Webster J. G., 1990, *Electrical Impedance Tomography*, Adam Hilger.
- Williams R. A. and Beck M. S., 1995, *Process Tomography : Principles, Techniques and Applications*, Butterworth-Heinemann, Oxford.
- Williams, R. A., Jia X., and McKee S. L., 1996, "Development of slurry mixing models using resistance tomography," *Powder Technology*, Vo. 87, pp. 21-27.
- Xie C. G., Huang S. M., Hoyle B. S., Thorn R., Lenn C., Snowden D., and Beck M. S., 1992, "Electrical capacitance tomography for flow imaging : system model for development of image reconstruction algorithms and design of primary sensors," *IEE Proc. G*, Vol. 139, No. 1, pp.89-98.
- Xie C. G., Reinecke N., Beck M. S., Mewes D., and Williams R. A., 1995, "Electrical tomography techniques for process engineering applications," *The Chemical Engineering Journal*, Vol. 56, pp. 127-133.
- Yorkey T. J., Webster J. G., and Tompkins W. J., 1987, "Comparing reconstruction algorithms for electrical impedance tomography," *IEEE Transactions on Biomedical Engineering*, Vol.34, No.11, pp.843-852.

감사의 말

2년 동안의 수확을 얻을 수 있도록, 해, 비, 바람 등과 같은 도움을 주신 많은 분께 감사의 인사를 드리며, 석사과정을 정리하고자 합니다.

오늘의 제가 있을 수 있도록 사랑과 믿음의 힘이 되어 주신 우리 식구들, 특히, 인내와 노력이라는 생활의 미덕을 일깨워 주신 아버지께 감사 드립니다.

모든 일에 있어 시간이 부족한 것이 아니라 의지가 부족하다는 깨달음을 주시고, 보다 나은 논문이 되도록 끝까지 지켜봐 주신 김경연 교수님께 존경과 감사를 드립니다. 그리고 바쁘신 가운데서도 논문심사를 통해 깨우침을 주신 도양희 교수님, 강민제 교수님께 깊은 감사를 드립니다. 또한, 관심을 갖고 도움을 주셨던 김경식 교수님, 고성택 교수님, 이광만 교수님께도 감사를 드립니다.

한국 과학 기술부의 원자력 기초과제인 “이상 유동장 가시화를 위한 ET 기법 개발”이라는 프로젝트를 함께 수행하며 많은 가르침을 주신 이윤준 교수님, 김민찬 교수님, 김신 교수님을 비롯한 여러 교수님들께 깊은 감사의 마음을 전합니다.

대학원 생활동안 망중한(忙中閑)의 여유를 함께 했던 졸업동기 성운오빠에게 감사를 전하며, HanTechSnS 식구들, 울 이쁜 후배 혜진, 은미, 은선에게도 감사함을 전합니다. 그리고, 아낌없는 조언과 충고를 해 주신 봉석오빠, 은성오빠, 영균오빠, 경훈선배님, 경희언니, 유신언니, 영아언니에게 감사의 마음을 전하며, 모든 분들께 앞날의 무한한 발전이 있으시길 바랍니다.

저의 이 작은 결실이 그분들께 조금이나마 기쁨이 되기를 바랍니다. 감사합니다.